J Mater Sci: Mater Med (2008) 19:797–803
DOI 10.1007/s10856-007-3213-4

# Structural characterization of zinc-substituted hydroxyapatite prepared by hydrothermal method

**Ming'Ou Li · Xiufeng Xiao · Rongfang Liu · Cuiyu Chen · Lizhong Huang**

Received: 7 February 2007 / Accepted: 6 June 2007 / Published online: 1 August 2007


**Abstract** Zinc-substituted hydroxyapatite (Zn-HA) powders were prepared by hydrothermal method using $Ca(NO_3)_2$, $(NH_4)_3PO_4$ and $Zn(NO_3)_2$ as reagents. X-ray fluorescence spectroscopy (XRF), X-ray diffraction (XRD), fourier transform infrared spectroscopy (FT-IR) and transmission electron microscopy (TEM) were used to characterize the crystalline phase, microstructure, chemical composition, morphology and thermal stability of Zn-HA. The results show that the substitution content of zinc (Zn) in Zn-HA powders prepared in NaOH solution is higher than that prepared in $NH_3$ solution, and is lower than that of the corresponding amount of starting materials. The substitution of the Zn ion for calcium ion causes a lower crystallinity of Zn-HA and changes the lattice parameters of Zn-HA, since the ionic radius is smaller in $Zn^{2+}$ (0.074 nm) than in $Ca^{2+}$ (0.099 nm). Furthermore, the substitution of the Zn ions restrains the growth of Zn-HA crystal and decreases the thermal stability of Zn-HA. Zn-HA powder prepared in $NH_3$ solution starts to decompose at 800 °C when the Zn fraction increases to 15 mol%, while that prepared in NaOH solution start to decompose at 5 mol% Zn. The substitution content of Zn significantly influences the thermal stability, microstructure and morphology of Zn-HA.

## Introduction

Hydroxyapatite (HA, $Ca_{10}(PO_4)_6(OH)_2$), a synthetic material analogous to calcium phosphate found in bone, is considered for orthopaedic and dental applications. This biomaterial implanted in human body leads to release of calcium and phosphate absorbed by human tissues and presents highly biocompatible and bioactive properties. However, the stability of crystal structure of HA is higher than that of natural apatite. HA is difficult to degrade in living body. Most natural apatite is non-stoichiometric because of the presence of minor constituents such as cations ($Mg^{2+}$, $Mn^{2+}$, $Zn^{2+}$, $Na^+$, $Sr^{2+}$) or anions ($HPO_4^{2-}$ or $CO_3^{2-}$) [1, 2]. Trace ions substituted in apatite can have an effect on the lattice parameters, the crystallinity, the dissolution kinetics and other physical properties of apatite [3–7]. Trace ions substituted HA can also improve its clinical applications, like $Zn^{2+}$ [8].

Zn, in particular, is essential for the development and growth of all species, including humans, and has been implicated with mineralization in biological systems. Zn is found in all human tissues, with bone containing the major part of total body [9] and closely related to bone metabolism [10]. Zn content ranges from 0.0126 wt% to 0.0217 wt% in human bone and is relatively higher than the average Zn content of whole fat-free adult tissues (0.0030 wt%) and that of plasma (12–17 Zn μM) [11–14]. The important role of Zn in many biological functions is well known: Zn is a cofactor for many enzymes and is essential for DNA replication. Zn stimulates animal bone growth and bone mineralization [15–17]. Zn has a direct effect on osteoblastic cells in vitro [18] and a potent inhibitory effect on osteoblastic bone resorption [19]. As is known, Zn can modify the production of cytokines [20]. The slow release of Zn incorporated into an implant material could promote bone formation around the implant and accelerate recovery of the patient. Many studies have demonstrated that Zn-HA significantly improved the bioactivity of HA [21–23]. Therefore, Zn-HA can be a new generation of materials for bone tissue engineering.

M. O. Li · X. F. Xiao · R. F. Liu (✉) · C. Y. Chen · L. Z. Huang
College of Chemistry and Materials Science, Fujian Normal University, Fuzhou 350007, China
e-mail: rfliu@vip.sina.com

The main methods of preparation of Zn-HA, which have been reported, are sol-gel procedure [21, 22, 24] and chemical precipitation [23, 25, 26]. But these products prepared by precipitation are irregular and easy to agglomerate, while those products prepared by sol-gel procedure have a low crystallinity. Hydrothermal methods [27], as the name implies, deal with the application of high temperatures to aqueous solutions to facilitate the precipitation of crystals of dimensions larger than those attainable using ordinary wet methods. Because the aqueous precipitating medium at atmospheric pressure has its boiling point as the upper temperature limit, being heated under high pressure enables this limit to be exceeded. In an autoclave, the desired high pressure is produced by the vapour of the solvent of the precipitating medium, because the system is subjected to a high temperature in a sealed enclosure. The principal advantage of such methods has been to enhance considerably the crystallinity and purity of the product.

The purpose of the present study is to prepare Zn-HA by hydrothermal technique and to study the difference of the substitution of Zn-HA with $NH_3$ aqueous solutions or NaOH solutions adjusting the pH, respectively. Additionally, microstructure, chemical composition, morphology and thermal stability of Zn-HA have been investigated.

## Materials and methods

### Preparation of Zn-HA powders

The pure HA and Zn-HA powders were prepared by hydrothermal method using $Ca(NO_3)_2$, $(NH_4)_3PO_4$, and $Zn(NO_3)_2$ aqueous solutions as reagents. The amount of reagents was listed in Table 1. The amount of regents was calculated on the assumption that Zn would substitute calcium. The Zn fraction for each composition was represented as $[Zn]/[Ca + Zn] \times 100$ (mol%). The pH of $Ca(NO_3)_2$ solution was kept higher than 10.0 and that of $(NH_4)_3PO_4$ solution was kept higher than 11.0 by the addition of $NH_3$ or NaOH solution, respectively. A 0.3 M $(NH_4)_3PO_4$ solution was added to $Ca(NO_3)_2$ and $Zn(NO_3)_2$ containing 0.2 g Polyethylene Glycol, and the reaction mixture was stirred for 0.5 h, then hydrothermal treatment at 200 °C for 8 h. The resulting precipitates were filtered, dried at 100 °C overnight. Additionally, a fraction of each as-prepared sample was treated at 400 °C or 800 °C for 1 h under air atmosphere, respectively. Zn-HA powders prepared by using $NH_3$ solution to adjust pH value were denoted as Zn-HA1, and those prepared by using NaOH solution to adjust pH value were denoted as Zn-HA2.

### Sample characterization

The Zn content in Zn-HA was determined by X-ray fluorescence (XRF) spectroscopy using a Philips Magix PW2424 spectrometer. Hitachi 600 Transmission electron microscopy (TEM) was employed to characterize the microstructure of HA and Zn-HA. The phase composition of as-prepared powders and the heated powders were determined by X-ray diffraction (XRD). Philips X'Pert MPD diffractometer with Cu *K*a radiation was used, the X-ray generator operated at 40 KV and 40 mA. Dataset were collected over the range of 10°–90° with a step size of 0.02° and a count rate of 3.0° /min. Phases identification was achieved by comparing the diffraction patterns of HA and Zn-HA with ICDD(JCPDS) standards. The average crystallite size of the samples was calculated by using the Scherrer formula. FT-IR spectra were obtained by using Nicolet Avatar 360 spectrometer. Spectra were obtained at 4 $cm^{-1}$ resolution averaging 64 scans.

## Results and discussion

### Morphology of products

The TEM micrographs of as-prepared powders are shown in Fig. 1. The addition of polyethylene glycol as surface agent makes Zn-HA1 nanoparticle better disperse. The Zn content has a negative effect on the crystal size, the mean value size decreases with Zn content increasing. Figure 1 shows that the pure HA is stick-shaped crystallites, however, more needle-shaped crystallites increase with Zn

**Table 1** Quantities of reactants used and the measured Zn mol% of the samples

| Samples | $n_{(NH4)3PO4}$/mol | $n_{Ca(NO3)2}$/mol | $n_{Zn(NO3)2}$/mol | Expected Zn mol/% | Measured Zn mol/% | Calculated chemical formula of Zn-HA |
|---|---|---|---|---|---|---|
| HA | 0.009 | 0.015 | 0 | 0 | – | $Ca_{10}(PO_4)_6(OH)_2$ |
| 10 mol%Zn-HA1 | 0.009 | 0.0135 | $1.5 \times 10^{-3}$ | 10 | 4.1 | $Ca_{9.59}Zn_{0.41}(PO_4)_6(OH)_2$ |
| 10 mol% Zn-HA2 | 0.009 | 0.0135 | $1.5 \times 10^{-3}$ | 10 | 8.5 | $Ca_{9.15}Zn_{0.85}(PO_4)_6(OH)_2$ |
| 20 mol% Zn-HA1 | 0.009 | 0.012 | $3.0 \times 10^{-3}$ | 20 | 9.3 | $Ca_{9.07}Zn_{0.93}(PO_4)_6(OH)_2$ |
| 20 mol% Zn-HA2 | 0.009 | 0.012 | $3.0 \times 10^{-3}$ | 20 | 16.4 | $Ca_{8.36}Zn_{1.64}(PO_4)_6(OH)_2$ |

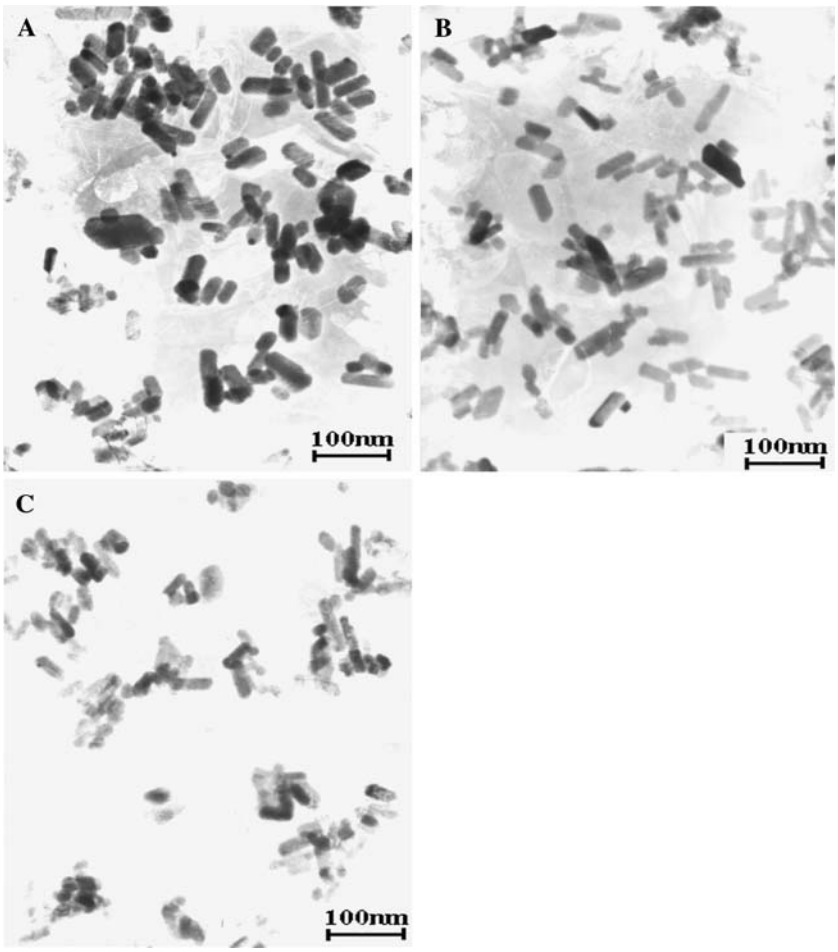


**Fig. 1** TEM images of Zn-HA1 powder prepared with different Zn fraction: (**A**) 0 mol%; (**B**) 5 mol%; (**C**) 10 mol%

content increasing. From the picture, the aggregate consisting of interconnected fine rod-like particles with about 50–60 nm in length and 20 nm in width are observed. The size of the apatite particles reduces with Zn content increasing. It also indicates that the crystallinity of the apatite decreases with Zn content increasing. In human body, the crystal size of apatite particle is about (5–20) × 60 nm. Therefore, to a certain extent, the size of Zn-HA1 prepared by hydrothermal matches natural HA.

## The substitution content of Zn

It has been reported that it is quite difficult for divalent cations such as $Zn^{2+}$, $Ni^{2+}$, $Mn^{2+}$ and $Cu^{2+}$ to replace $Ca^{2+}$ in the apatite structure [28]. The results of the chemical analysis by XRF of the 10 mol% Zn-HA1, 10 mol% Zn-HA2, 20 mol% Zn-HA1 and 20 mol% Zn-HA2 powders were listed in Table 1. The Zn contents of samples are lower than those of the corresponding amount of starting material. It implies that some of Zn ions remain in the mother solution after precipitation. However, the substitution content of $Zn^{2+}$ for $Ca^{2+}$ in HA powders prepared by chemical precipitated is almost equal to starting material [25], indicating that the substitution of $Zn^{2+}$ into HA structure through hydrothermal method is more difficult than that through chemical precipitation. The measured Zn content of 10 mol% and 20 mol% Zn-HA2 is twice as large as 10 mol% and 20 mol% Zn-HA1. It demonstrated that Zn ions are easier to be substituted into the crystal structure of HA with NaOH adjusting the pH. The reason could be that: $Zn(NH_3)_4{}^{2+}$ was generated by using $NH_3$ to adjust the pH, while $Zn(OH)_2$ was created by NaOH. $Zn(NH_3)_4{}^{2+}$ is more stable than $Zn(OH)_2$ and is more difficult to release $Zn^{2+}$. Thus, a great many Zn ions remain in the solution after precipitation.

## XRD analysis

X-ray diffraction patterns of as-prepared and heat-treated powders were showed in Figs. 2–6. Figures 2 and 3 show the XRD patterns of Zn-HA1 and Zn-HA2 powder with various Zn fractions. The peaks assigned to the apatite structure just matches the ICDD standard for HA (JCPDS 09-0432), when the Zn fraction is below 20 mol%.

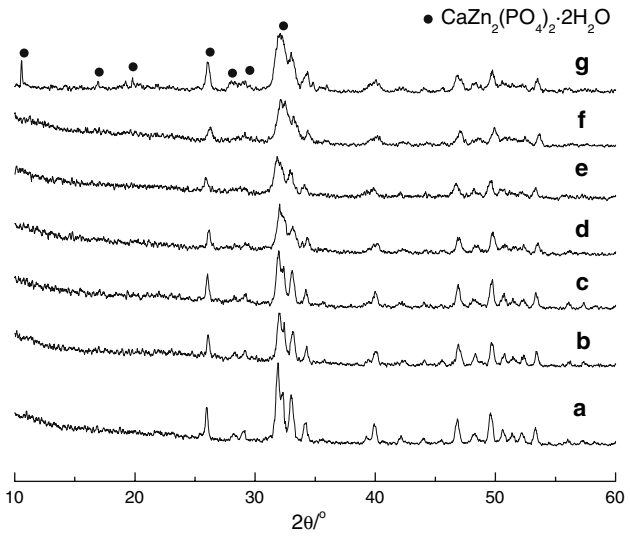


**Fig. 2** XRD patterns of Zn-HA1 powder prepared with different Zn fractions. (**a**) 0 mol%, (**b**) 3 mol%, (**c**) 5 mol%, (**d**) 10 mol%, (**e**) 15 mol%, (**f**) 20 mol%, (**g**) 40 mol%

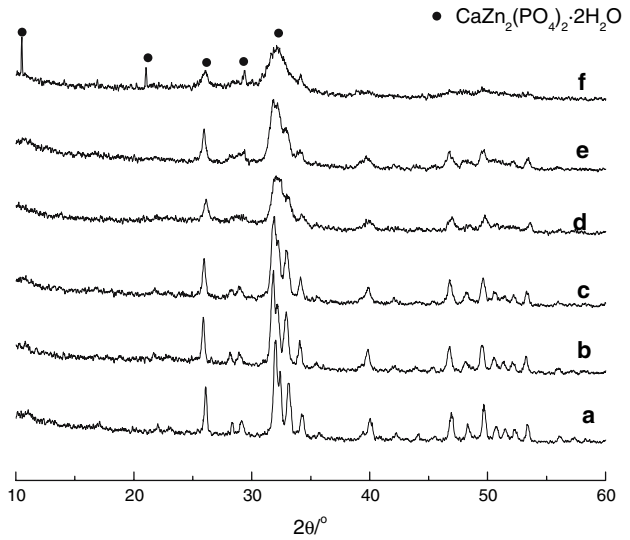


**Fig. 3** XRD patterns of Zn-HA2 powder prepared with different Zn fractions using NaOH controlling pH value. (**a**) 0 mol%, (**b**) 5 mol%, (**c**) 10 mol%, (**d**) 15 mol%, (**e**) 20 mol%, (**f**) 40 mol%

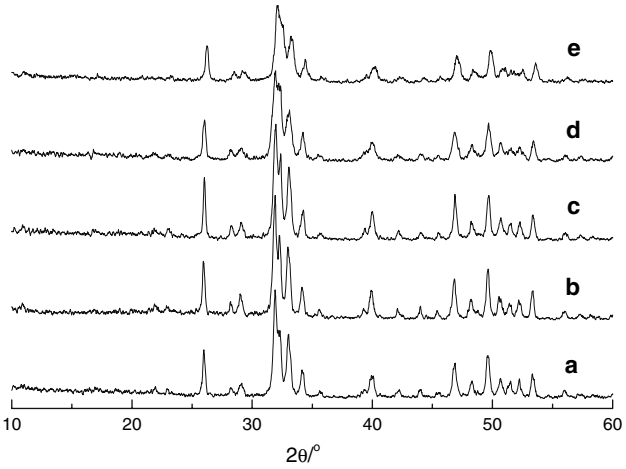


**Fig. 4** XRD patterns of Zn-HA1 heat-treated at 400 °C for 1 h (**a**) 0 mol%, (**b**) 3 mol%, (**c**) 5 mol%, (**d**) 10 mol%, (**e**) 15 mol%

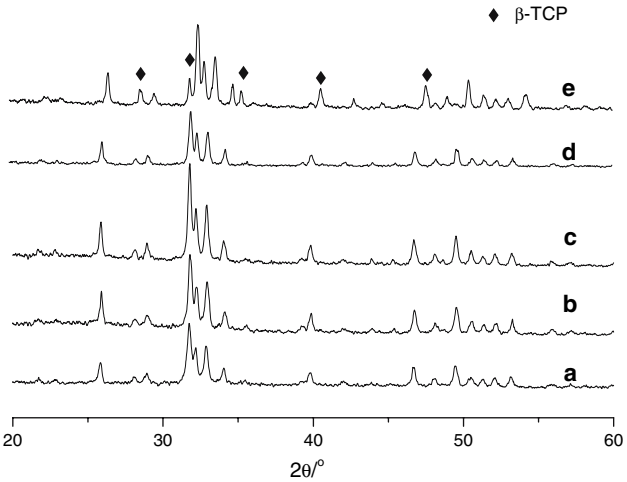


**Fig. 5** XRD patterns of Zn-HA1 heat-treated at 800 °C for 1 h. (**a**) 0 mol%, (**b**) 3 mol%, (**c**) 5 mol%, (**d**) 10 mol%, (**e**) 15 mol%

However, these diffraction peaks become wider and less intense as the Zn content increases. There could be some reasons: (1) the ionic radius is smaller in $Zn^{2+}$ (0.074 nm) than in $Ca^{2+}$ (0.099 nm); (2) it also could be the result of the effect of crystal size. The observation of TEM and calculation by Scherrer formula prove that the crystallite size decreases with the Zn content increasing; (3) it could be the result that the crystallinity of the apatite significantly decreases. On the other hand, the calcium zinc phosphate hydrate ($CaZn_2(PO_4)_2{\cdot}2H_2O$) phase appears in addition to the low-crystalline apatite phase when the Zn fraction is 40 mol%. With increasing of Zn fraction, the peak intensity of the calcium zinc phosphate hydrate increases, and that of the apatite decreases. The peak intensity of Zn-HA2 is higher than that of Zn-HA1, indicating that the crystals have higher crystallinity in NaOH solution than that in $NH_3$ solution.

Figure 4 shows the XRD patterns of Zn-HA1 powder heat-treated at 400 °C for 1 h. All the specimens treated at 400 °C show that the diffraction peaks are ascribed to the apatite only. Almost no visible change was appreciable in the XRD patterns. These patterns show that the diffraction peaks are narrower than those of as-prepared samples, pointing out larger crystallites and higher crystallinity. It indicates that the crystal size and the crystallinity of the apatite significantly increase after heating. Furthermore,

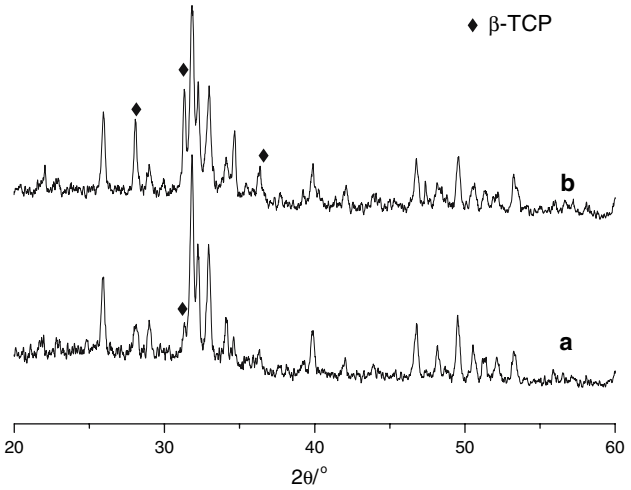


**Fig. 6** XRD patterns of Zn-HA2 heat-treated at 800 °C for 1 h. (**a**) 5 mol%, (**b**) 10 mol%

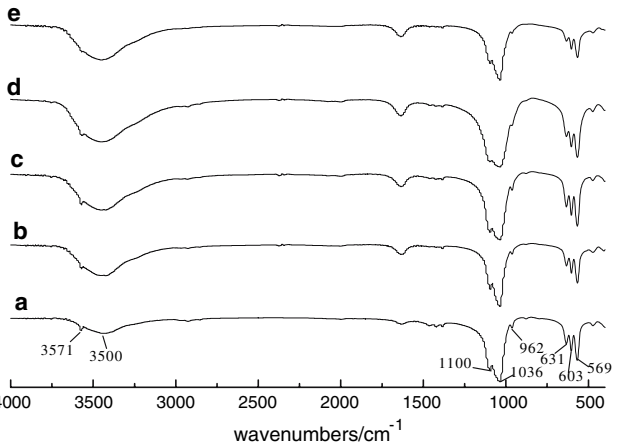


**Fig. 7** FT-IR spectra of Zn-HA1 powder with different Zn fractions. (**a**) 0 mol%, (**b**) 3 mol%, (**c**) 5 mol%, (**d**) 10 mol%, (**e**) 15 mol%

the patterns with no secondary phases, such as TCP or CaO are detected.

Figures 5 and 6 show the XRD patterns of Zn-HA1 and Zn-HA2 powders heat-treated at 800 °C for 1 h. As shown in Fig. 5, $\beta$-calcium phosphate ($\beta$-TCP) phase appears when Zn fraction increases to 15 mol%. It indicates that the Zn-HA was transformed into Zn-substituted TCP after the heat treatment at 800 °C [28]. As shown in Fig. 6, $\beta$-TCP phase appears when Zn fraction only up to 5 mol%, the peaks of $\beta$-TCP phase increase with the Zn fraction increasing. It shows that the amount of Zn which is incorporated into HA lattice influences the thermal stability of HA. The thermal stability of Zn-HA decreases with Zn fraction increasing. Comparing Fig. 5 with Fig. 6, we can see that 15 mol% Zn-HA1 begins to decompose, while 5 mol% Zn-HA2 begins to decompose. The reason is that the substitute content of Zn with NaOH solution adjusting the pH is higher than that with $NH_3$ aqueous solution. In other words, the thermal stability of HA decreases with Zn content increasing.

## FT-IR analysis

Figure 7 shows the FT-IR spectra of Zn-HA1 powder with various Zn fractions. All of them show the characteristic absorption bands of HA. The bands at 3571 $cm^{-1}$ and 631 $cm^{-1}$ correspond to the stretching and vibrational modes, respectively, of the hydroxyl group. However, the stretching vibration mode of OH– is lower than the OH– (3644 $cm^{-1}$) of $Ca(OH)_2$, which indicates that a weak hydrogen-bonding exists between OH– and $PO_4^{3-}$ or OH– and OH–. But in the crystal structure of HA, the distance between OH– and OH– is 0.344 nm, and it is unable to generate hydrogen-bonding between them, while it is able to create hydrogen-bonding between OH– and $PO_4^{3-}$, because the distance of O(H)–O is 0.3068 nm [29]. Gonzalez-Diaz had approved the deduction [30]. Hence, the stretching vibration modes of OH- are lower, which was caused by the hydrogen-bonding created by oxygen between OH– and $PO_4^{3-}$. The intense bands at 1100, 1036, and 962 $cm^{-1}$ correspond to P–O stretching vibration modes, whereas the doublet at 603–569 $cm^{-1}$ corresponds to the O–P–O bending mode. Finally, the broad band at 3500 $cm^{-1}$, as well as the band centred at 1653 $cm^{-1}$, corresponds to $H_2O$ adsorbed on the surface. With increasing Zn fraction, the separation of three $PO_4^{3-}$ stretching peaks (962, 1036 and 1100 $cm^{-1}$) become obscure, and the OH bending peak at 631 $cm^{-1}$ do broaden. These changes suggest that the crystallinity of the apatite decreased as Zn fraction increase, which agree with the results of the XRD patterns.

The FT-IR spectra of heat-treated HA and Zn-HA1 powders, as shown in Fig. 8, show no significant changes from the as-prepared samples. The broad IR peak around 3500 $cm^{-1}$ became smaller after the heat treatment at 400 °C. The result reflects the decrease in amounts of the adsorbed and lattice $H_2O$.

## Lattice parameters

Hydroxyapatite monocrystals adopt a needle shape and are oriented following the $c$-axis of the hexagonal HA structure, $a$-axis of the hexagonal HA structure parallel with any one side of hexagon [31]. The observed peak position in $2\theta$ was determined by full width at half maximum (FWHM). The average crystallite size of the samples was calculated using the Scherrer formula [31]:

$$D_{(hkl)} = \frac{k\lambda}{\cos\theta\sqrt{\omega^2 - \omega_0^2}}$$

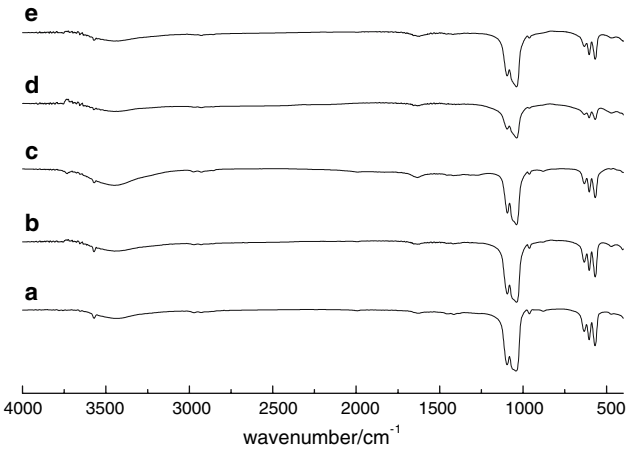


**Fig. 8** FT-IR spectra of Zn-HA1 powder heated-treated at 400 °C for 1 h. (**a**) 0 mol%, (**b**) 3 mol%, (**c**) 5 mol%, (**d**)10 mol%, (**e**)15 mol%

**Table 2** The size of crystal grains of the products with various Zn fractions

| Sample | Size of crystal grain of HA and Zn-HA /nm | |
|---|---|---|
| | *a*-axis | *c*-axis |
| HA | 29.9 | 41.2 |
| 5 mol% Zn-HA1 | 21.0 | 69.1 |
| 10 mol% Zn-HA1 | 20.9 | 58.7 |

where $D_{(hkl)}$ is the crystallite size (nm); $k$ is the shape coefficent, 0.9; $\lambda$ is the wave length(nm); $\theta$ is the diffraction angle(°); $\omega$ corresponds to experimental FWHM obtained for each sample; $\omega_0$ corresponds to standard FWHM values. For this purpose, we choose the FWHM at (002) ($2\theta = 25.8°$) and (300) ($2\theta = 32.9°$) to calculate the crystal size along with the $c$ crystallographic axis and $a$ crystallographic axis, respectively. We have used the LaB6 (SRM 660-National Institute of Standard Technology) powder standard pattern to determine the instrumental width (0.087) and afterward to calculate the crystalline size via the Scherrer formula. The results are shown in Table 2. As Zn content increases, the crystal size of *a*-axis decreases and that of *c*-axis increases; these tendencies are consistent with the results of the TEM observation.

The ionic radius is smaller in $Zn^{2+}$ (0.074 nm) than that in $Ca^{2+}$ (0.099 nm), which must be affected by the crystal structure of HA. The effect of the Zn substitution on the crystal structure of HA was determined by Rietveld structure refinement of the X-ray diffraction data. The most important structure parameters are the lattice parameters and unit cell volume, which were shown in Table 3. The lattice parameter *a* decreased with increasing Zn fraction up to 10 mol%, increased over 10 mol% Zn. The lattice parameter *c* monotonously decreased with increasing Zn fraction. Such contraction in *a, c* may reflect the smaller ionic radius in $Zn^{2+}$ (0.074 nm) than in $Ca^{2+}$ (0.099 nm). It has been previously reported that Zn-substitution for Ca sites in the apatite structure increases the lattice parameters *a, c* [31]. The present work clearly shows the opposite tendency to that report. However, we have the similar tendency to Miyaji [25] who had reported that the lattice parameter *a* decreased up to 5 mol% Zn, and started to increase over 5 mol% Zn. The lattice parameter *c* monotonously decreases with Zn fraction increasing. As remarked above, Zn ions are more difficult substitution into the crystal structure of HA through hydrothermal method than that through chemical precipitation. The fraction of Zn incorporated into the crystal structure of HA is lower through hydrothermal method than that through chemical precipitation. Hence, the lattice parameter *a* decreases with Zn fraction up to 10 mol%, increased over 10 mol% Zn.

**Table 3** Lattice parameters of the products with various Zn fractions

| Sample | *a*/nm | *c*/nm | Unit cell volume/nm$^3$ |
|---|---|---|---|
| HA | 0.939579 | 0.684957 | 0.52367 |
| 3 mol% Zn-HA1 | 0.938242 | 0.684445 | 0.52179 |
| 5 mol% Zn-HA1 | 0.938066 | 0.684225 | 0.52143 |
| 10 mol% Zn-HA1 | 0.936287 | 0.683966 | 0.51915 |
| 15 mol% Zn-HA1 | 0.939274 | 0.683737 | 0.52240 |
| 20 mol% Zn-HA1 | 0.940666 | 0.683667 | 0.52390 |

## Conclusion

Zn-HA powders were successfully prepared by hydrothermal method using $Ca(NO_3)_2$, $(NH_4)_3PO_4$ and $Zn(NO_3)_2$ as reagents, but the substitute contents of Zn into HA structure are lower than those of the corresponding amount of starting material. The substitution of $Zn^{2+}$ into HA structure through hydrothermal method is more difficult than that through chemical precipitation. The crystallinity and the substitution contents of Zn of Zn-HA prepared with NaOH solution adjusting pH value are higher than that prepared by $NH_3$ aqueous solution adjusting pH value. The crystallinity and the thermal stability of the apatite significantly decrease with Zn fraction increasing. The lattice parameter *a* decreases with Zn fraction up to 10 mol% Zn, but starts to increase over 10 mol% Zn. The lattice parameter *c* monotonously decreases with Zn fraction increasing.

**Acknowledgements** The authors would like to thank National Nature Science Foundation of China (30600149), the science research foundation of ministry of Health & United Fujian Provincial Health and Education Project for Tackling the Key Research, P.R. China (WKJ 2005-2-008), Fujian Development and Reform Commission of China (No. 2004[477]) and Undergraduate extracurricular project of Fujian Normal University (BKL2006-021).

## References


1. I. MAYER and J. D. B. FEATHERSTONE, *J. Cryst. Growth* **219** (2000) 98
2. S. BEN ABDELKADER, I. KHATTECH, C. REY and M. JEMAL, *Thermochim. Acta.* **376** (2001) 25
3. G. DACULSI, R. Z. LEGEROS, M. HEUGHEBAERT and I. BARBIEUX, *Calcif. Tissue Int.* **46** (1990) 20
4. I. R. GIBSON, K. A. HING, J. D. REVELL, J. D. SANTOS, S. M. BEST and W. BONFIELD, *Key Eng. Mater.* **203** (2002) 218
5. M. OKAZAKI, *Biomaterials* **16** (1995) 703
6. I. R. GIBSON and W. Bonfield, *J. Biomed. Mater. Res.* **59** (2002) 697
7. E. BERTONI, A. BIGI, G. COJAZZI, M. GANDOLFI, S. PANZAVOLTA and N. ROVER, *J. Inorg. Biochem.* **29** (1998) 72
8. R. Z. LEGEROS and J. P.LEGROS, in "Phosphate Minerals", Edited by J. O. NRIAGU and P. B. MOORE (Springer-Verlag, New York, 1984) p. 351
9. E. JALLOT, J. L. IRIGARAY, H. OUDADESSE, V. BRUN, G. WEBER and P. FRAYSSINET, *Eur. Phys. J. App. phys.* **6** (1999) 205
10. J. H. BEATTIE and A. ALISON, *Nutr. Res. Rev.* **5** (1992) 1672
11. E. J. UNDERWOOD, in "Trace Elements in Human and Animal Nutrition" (Academic Press, London, 1977) p. 196
12. E. I. HAMILTON, M. J. MINSKI, J. J. CLEARY, *Sci. Total Environ.* **1** (1972/1973) 341
13. WHO Expert Committee, *WHO Tech. Rep. Ser.* **532** (1973) 9
14. W. J. BETTGER and B. L. O'DELL, *J. Nutr. Biochem.* **4** (1993) 194
15. M. YAMAGUCHI, K. INAMOTO and Y. E. SUKETA, *Res. Exp. Med.* **186** (1986) 337
16. M. YAMAGUCHI, H. OISHI and Y. SUKETA, *Biochem. Pharmacol.* **36** (1987) 4007
17. M. YAMAGUCHI, H. OISHI and Y. SUKETA, *Biochem. Pharmacol.* **37** (1988) 4075
18. M. HASHIZUME and M. YAMAGUCHI, *Mol. Cell. Biochem.* **122** (1993) 59
19. S. KISI, M. YAMAGUCHI, *Biochem. Pharmacol.* **48** (1994) 1225
20. B. BAO, A. S. PRASAD, F. W. BECK and M. GODMERE, *Am. J. Physiol. Endocrinol. Metab.* **285** (2003) E1095–102
21. A. GRANDJEAN-LAQUERRIERE, P. LAQUERRIERE, E. JALLOT, J. M. NEDELEC, M. GUENOUNOU and D. LAURENT-MAQUIN, *Biomaterials* **27** (2006) 3195
22. E. JALLOT, J. M. NEDELEC, A. S. GRIMAULT, E. CHASSOT, A. GRANDJEAN-LAQUERRIERE, P. LAQUERRIERE and D. LAURENT-MAQUIN, *Colloids Surf. B Biointerfaces* **42** (2005) 205
23. E. FUJII, M. OHKUBO, K. TSURU, S. HAYAKAWA, A. OSAKA, K. KAWABATA, C. BONHOMME and F. BABONNEAU, *Acta Biomaterialia.* **2** (2006) 69
24. S. D. MIAO, W. J. WENG, K. CHENG, P. Y. DU, G. SHEN, G. R. HAN and S. ZHANG, *Surf. Coat. Technol.* **198** (2005) 223
25. F. MIYAJI, Y. KONO and Y. SUYAMA, *Mater. Res. Bull.* **40** (2005) 209
26. R. Z. LEGEROS, C. B. BLEIWAS, M. RETINO, R. ROHANIZADEH and J. P. LEGEROS, *Am. J. Dent.* **12** (1999) 65
27. W. L. JOLLY, in "The Synthesis and Characterization of Inorganic Compounds" (Prentice Hall, Englewood Cliffs, NJ, 1970) p. 231
28. A. ITO, K. OJIMA, H. NAITO, N. ICHINOSE and T. TATEISHI, *J. Biomed. Mater. Res.* **50** (2000) 178
29. C. B. BADDIELANG and E. E. Berry, *J. Spectro. Chim. Acta.* **22** (1996) 1407
30. P. F. GONZALEZ-DIAZ and M. SANDTOS, *J. Solid State Chem.* **22** (1997) 193
31. E. BOUYER, F. GITZHOFER, I. BOULOS, *J. Mater. Sci., Mater. Med.* **11** (2000) 523